PAPER

Check for updates

BODIPY–pyrene donor–acceptor sensitizers for triplet–triplet annihilation upconversion: the impact of the BODIPY-core on upconversion efficiency†

Natalia Kiseleva,[a] Mikhail A. Filatov, [ID][b] Jan C. Fischer,[a] Milian Kaiser,[a] Marius Jakoby,[a] Dmitry Busko,[a] Ian A. Howard, [ID][ac] Bryce S. Richards [ID] *[ac] and Andrey Turshatov [ID] *[a]

Triplet–triplet annihilation upconversion (TTA-UC) is an important type of optical process with applications in biophotonics, solar energy harvesting and photochemistry. In most of the TTA-UC systems, the formation of triplet excited states takes place *via* spin–orbital interactions promoted by heavy atoms. Given the crucial role of heavy atoms (especially noble metals, such as Pd and Pt) in promoting intersystem crossing (ISC) and, therefore, in production of UC luminescence, the feasibility of using more readily available and inexpensive sensitizers without heavy atoms remains a challenge. Here, we investigated sensitization of TTA-UC using BODIPY–pyrene heavy-atom-free donor–acceptor dyads with different numbers of alkyl groups in the BODIPY scaffold. The molecules with four and six alkyl groups are unable to sensitize TTA-UC in the investigated solvents (tetrahydrofuran (THF) and dichloromethane (DCM)) due to negligible ISC. In contrast, the dyad with two methyl groups in the BODIPY scaffold and the dyad with unsubstituted BODIPY demonstrate efficient intersystem crossing (ISC) of 49–58%, resulting in TTA-UC with quantum yields of 4.7% and 6.9%, respectively. The analysis of the elementary steps of the TTA-UC process indicates that heavy-atom-free donor–acceptor dyads are less effective than their noble metal counterparts, but may equal them in the future if the right combination of solvent, donor–acceptor sensitizer structure, and new luminescent molecules as TTA-UC emitters can be found.

Introduction

Anti-Stokes luminescence based on triplet–triplet annihilation upconversion (TTA-UC) has recently attracted much interest in various applications such as biophotonics,[1–5] photovoltaics,[6–9] photochemistry,[10–14] production of solar fuels,[15] and anticounterfeiting.[16] There are two underpinning reasons motivating TTA-UC research. First, recent studies have demonstrated a wide variety of TTA-UC systems – from purely organic to hybrid organic/inorganic materials – which leads to many options for their application.[17] Second, TTA-UC provides

broader and stronger absorption[18] as well as affords efficient UC luminescence under lower light intensities[19–22] when compared to other prominent UC systems based on lanthanide ions.[23,24]

The typical process of TTA-UC is illustrated in Fig. 1a. After absorption of a photon, the sensitizer undergoes intersystem crossing (ISC). The generated triplet state (localized on the sensitizer) transmits energy to a triplet state of an emitter molecule *via* triplet–triplet energy transfer (TTET). When two emitter molecules meet, triplet–triplet annihilation (TTA) occurs and results in the occupancy of an excited singlet state of one emitter; thus, the maximum possible quantum yield of the UC process is 50%. The emitter then undergoes radiative relaxation, emitting a new photon with an energy greater than the energy of the absorbed photons.

Benchmark TTA-UC systems are based on Pd and Pt-porphyrin sensitizers,[25] enabling very high ISC. When combined with organic emitter molecules like diphenylanthracene (DPA),[26] perylene,[27] and rubrene,[28] they afford uncorrected TTA-UC quantum yields (ϕ_{UC}) of 22%, 38%, and 8%, respectively. The correction of multiplying the ϕ_{UC} by a factor of 2 (given the

a Institute of Microstructure Technology, Karlsruhe Institute of Technology, Hermann-von-Helmholtz-Platz 1, 76344, Eggenstein-Leopoldshofen, Germany. E-mail: bryce.richards@kit.edu, andrey.turshatov@kit.edu

b School of Chemical and Pharmaceutical Sciences, Technological University Dublin, City Campus, Grangegorman, Dublin 7, Ireland

c Light Technology Institute, Karlsruhe Institute of Technology, Engesserstrasse 13, 76131 Karlsruhe, Germany

† Electronic supplementary information (ESI) available: Luminescence and UC luminescence transients, transient absorption spectra, and dependencies of UC luminescence on excitation intensity. See DOI: 10.1039/d1cp05382e
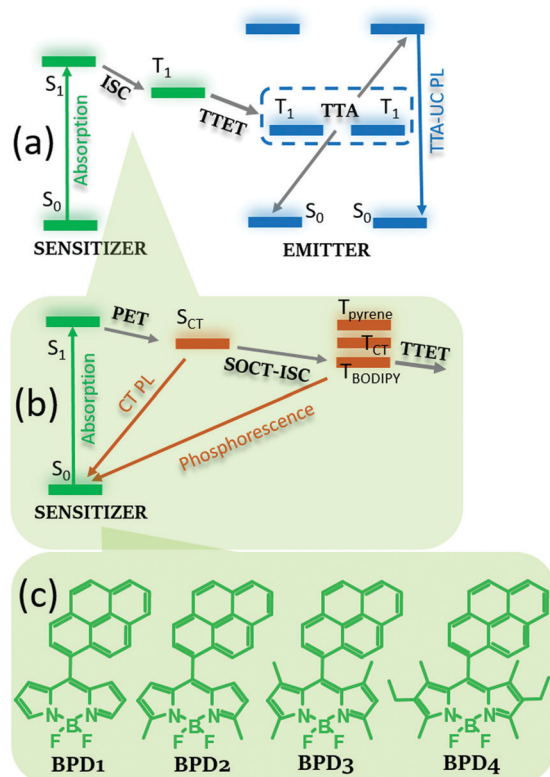
Fig. 1 (a) Generalized Jablonski diagram illustrating the TTA-UC process. Briefly, sensitizers absorb photons, giving rise to excited singlet states (S_1). The S_1 states undergo spin−orbit coupling intersystem crossing (SO-ISC) resulting in triplet states (T_1). Further, the triplet states of the emitter are populated *via* triplet−triplet energy transfer (TTET). Two triplet states relax *via* triplet−triplet annihilation giving rise to excited singlet states of the emitter, which emits photons with shorter wavelengths than those of the absorbed photons; (b) the ISC process with a heavy-atom-free sensitizer *via* photoinduced electron transfer (PET) giving rise to a charge transfer state (S_{CT}) and spin−orbit charge transfer intersystem crossing (SOCT-ISC) leads to triplet states (T_{CT} and T_{BODIPY}). The S_{CT} state can be emissive in polar solvents at room temperature (CT PL), whereas T_{CT} and T_{BODIPY} can emit (phosphorescence) at temperatures < 140 K; (c) heavy-atom-free BODIPY−pyrene (BPD 1−4) sensitizers with different BODIPY-cores.

theoretical UC limit of 50%) is somewhat commonplace in the literature; however, according to recent recommendations[29–31] such multiplication should be avoided.

In addition to the metalloporphyrins, 4,4-difluoro-4-*bora*-3*a*,4*a*-diaza-*s*-indacene (BODIPY) derivatives bearing iodine atoms[32] also proved to be popular sensitizers.[33] In the case of the metalloporphyrins and the BODIPY derivatives, the presence of Pt, Pd, and I enhances ISC due to the spin−orbit interaction (heavy-atom effect).[34] Many other new sensitizers have been studied over the past few years including quantum dots,[35–40] perovskite nanocrystals and films,[41–45] lanthanide complexes,[46] molecules showing TADF (thermally activated delayed fluorescence),[47–49] and electron donor−acceptor dyads.[50–56]

Among these classes of photosensitizers, heavy-atom-free donor−acceptor dyads are of particular interest for a new generation of TTA-UC systems. To promote the formation of long-lived triplet excited states, the BODIPY unit is combined with electron-donating aromatic subunits, such as anthracene,[57] phenoxazine,[53] perylene,[52] and pyrene.[58] Intramolecular electron transfer in these dyads leads to efficient formation of triplet excited states by SOCT-ISC. As it is indicated in Fig. 1b, the lowest singlet excited state of the sensitizer transforms into a charge transfer (CT) state, which further undergoes radiative/non-radiative decay or charge recombination into the lowest triplet excited state (SOCT-ISC). Usually, this process leads to population of the triplet state localized on the BODIPY subunit (^{3}BODIPY) with an energy in the range of 1.58–1.69 eV[53,54] that, for instance, is sufficient to enable TTET to the triplet state of the perylene emitter having an energy of 1.53 eV,[59] but is insufficient for TTET to DPA (another effective TTA-UC emitter) with an energy of 1.72 eV.[60]

We recently demonstrated that the BODIPY–pyrene dyad (BPD1, Fig. 1c) together with perylene in THF exhibits a high ϕ_{UC} of 6.9%,[31] which is among the highest values obtained for heavy-atom-free sensitizers so far. For example, a BODIPY–anthracene dyad paired with perylene as an emitter exhibited ϕ_{UC} up to 15.8% in dichloromethane (DCM)[50] and a group of BODIPY–phenoxazine dyads exhibited UC luminescence in a nonpolar solvent (hexane) with a ϕ_{UC} of 12.3%[53] (note that all data for ϕ_{UC} in ref. 50 and 53 should be divided by 2 as they were given with an additional factor of 2).

Furthermore, we observed a strong correlation between ϕ_{UC} and the solvent polarity (quantified *via* parameter $E_T(30)$[61]). We found the highest ϕ_{UC} of 6.9% for the BPD1 sensitizer in THF with $E_T(30) = 37.4$, whereas in less polar (toluene, $E_T(30) = 33.9$) and more polar (DCM, $E_T(30) = 42.2$) solvents the quantum yields are reduced down to 1.4% and 2.5%, respectively, although the reason for this peak-like behaviour is not clear. Moreover, the highest ϕ_{UC} of 6.9% obtained with perylene as the emitter is much lower than the theoretical TTA-UC limit of 50%, which also needs to be rationalized.

To understand the aforementioned results, herein we performed a more detailed study of corresponding TTA-UC systems in order to determine the efficiencies of the elementary steps of the TTA-UC process which contribute to the integral value of ϕ_{UC} (eqn (1)):

$$\phi_{UC} = 0.5 \times \phi_{ISC} \times \phi_{TTET} \times f_{TTA} \times \phi_{TTA} \times \phi_F \quad (1)$$

where ϕ_{ISC} denotes the efficiency of intersystem crossing, ϕ_{TTET} is the efficiency of triplet−triplet energy transfer, f_{TTA} is the spin statistical factor representing the fraction of triplet−triplet annihilation that results in a singlet state, excitation intensity dependent ϕ_{TTA} represents the fraction of triplets relaxing *via* bimolecular triplet−triplet annihilation (whereas the rest of the triplets relax to the ground *via* monomolecular processes), and ϕ_F denotes the quantum yield of the emitter (perylene).

We investigated the effect of the number of alkyl substituents in the BODIPY scaffold (Fig. 1c) on the ability to sensitize TTA-UC in DCM and THF. Furthermore, we applied methods of transient absorption and transient and variable-temperature photoluminescence (PL) spectroscopy to assess the efficiency of ISC, TTET and TTA for BPD sensitizers in solvents of different

polarity in order to identify the limiting step of TTA-UC sensitized using this donor–acceptor dyad.

Experimental

Chemicals

Deoxygenated tetrahydrofuran (THF) and dichloromethane (DCM) were purchased from Sigma-Aldrich (Merck). Compounds BPD 1–4 were prepared following a previously published procedure.[62]

Preparation of samples for UC measurements

The UC-systems (BPDs – perylene) in deoxygenated solvents were prepared inside a N_2-filled glovebox (GS Glovebox Systemtechnik GmbH) with a concentration of oxygen less than 0.1 ppm. The solutions were placed in a quartz cuvette and sealed inside the glovebox with a plastic cap and two layers of a sealing tape (Parafilm "M").

Photoluminescence characterization

The ultraviolet-visible (UV-vis) absorption spectra were recorded using a spectrophotometer (PerkinElmer Lambda 950). Steady-state PL spectra in THF and DCM were measured with 355 nm excitation (the third harmonic of an actively Q-switched laser (Innolas picolo-AOT MOPA)). Steady-state PL spectra in ethanol in the temperature range of 40–300 K were recorded using a closed-cycle cryostat (Oxford Instruments Optistat Dry TLEX) and a temperature-stabilized laser diode (Roithner LaserTechnik, 405 nm). The absolute quantum yields (ϕ_F) of perylene in DCM and THF were determined using a previously-described technique,[31] with a 3-port integrating sphere (CSTM-QE-060-SL, Labsphere, diameter of $\varnothing$ 15 cm). The first port ($\varnothing$ 0.6 cm) was used as the laser (the temperature stabilized laser diode, 405 nm) entrance, while the second port ($\varnothing$ 0.3 cm in diameter) was used for detection of luminescence with a fibre-coupled irradiance calibrated CCD spectrometer (AvaSpec-ULS2048x64-TEC, Avantes Inc.). A sample holder with the sample to be investigated was inserted through the third ($\varnothing$ 5.1 cm) port. The ϕ_F value was estimated as the ratio between the numbers of emitted and absorbed photons.

TTA-UC PL characterization

The steady-state UC spectra were measured using a custom-built optical system. A Ti:sapphire laser with an external doubling unit (Solstis + ECD-X, M-Squared Ltd) with a wavelength of 498 nm was used as the excitation source. The UC luminescence signal was recorded using a spectrometer (Avantes, AvaSpec-ULS2048 × 64TEC) and a slightly tilted notch-filter (NF03-532E-25, Semrock) to reject scattered excitation light.

The ϕ_{UC} value was calculated using the relative method according to a previously reported procedure.[31] Briefly, the luminescence from the CT state of BPD1, which is independent of oxygen presence and emitter (perylene) concentration, was used as a reference with ϕ_{ref} = 7.0% in DCM and ϕ_{ref} = 8.0% in THF. Using the relative method, the ϕ_{UC} value was calculated using eqn (2):

$$\phi_{UC} = \phi_{ref}(A_{ref}/A_{UC})(E_{UC}/E_{ref})(n_{UC}/n_{ref})^2 \qquad (2)$$

where ϕ denotes the quantum yield, A is the absorbance at the excitation wavelength, E represents the integrated luminescence intensity for all UC light and the reference emission peak, and n is the refractive index of a solvent at the emission wavelength. The indices UC and ref denote the sample and reference, respectively.

PL transient characterization

For UC PL lifetime measurements (µs time-scale), a multi-channel scaling (MCS) card (TimeHarp 260, PicoQuant) was used. The laser modulation was performed to achieve a regime with 5 ms laser on and 5 ms laser off (100 Hz, 50% duty cycle). The modulation of the 525 nm laser diode (Roithner Laser-Technik) was performed using a built-in function generator in the laser diode driver. To detect the rise and fall times of the UC emission, the transistor–transistor logic (TTL) signal from the laser diode controller was delayed by the use of a delay generator (DG645, Stanford Research Systems). The intensity of the laser was measured without the applied modulation. The spectral separation of the photoluminescence was achieved with a double monochromator (DTMS300, Bentham) and the emission at a specific wavelength was detected via a photo-multiplier tube (R928P, Hamamatsu), mounted in temperature-cooled housing (CoolOne, Horiba). A more detailed description of the experimental setups for measurements of steady-state and time resolved UC spectra, as well as ϕ_{UC}, can be found in previous publications.[31,51]

PL lifetimes on the ns time-scale were measured with a streak camera system. The third harmonic of an actively Q-switched laser (Innolas picolo-AOT MOPA) with a wavelength of 355 nm, a repetition rate of 1 kHz, and a pulse length of 500 ps was used as the excitation source. The streak camera (Hamamatsu Universal Streak Camera C10910) was used in the single-sweep mode to allow for a time-base of 20 ns and an instrumental-response function width of 310 ps. The PL kinetics were measured with an excitation fluence of 120 nJ cm^{-2}.

Transient absorption characterization

Transient absorption (TA) spectra were recorded by using a custom-built pump–probe setup with a resolution of $\sim$500 ps. Pump pulses (355 nm, 1 kHz) were provided by the third harmonic of an actively Q-switched Nd:YVO laser (Innolas picolo-AOT MOPA). White light continuum pulses (450–1000 nm) were generated by pumping a 2 mm thick sapphire crystal using the output of a commercial femtosecond laser (Light Conversion Pharos, 1030 nm, 10 µJ, 2 kHz, 260 fs). The white light pulses were dispersed onto a linear CCD image sensor and read out at 2 kHz. The adjacent spectra correspond to the transmission of the sample with and without the pump pulse and were used to calculate $\Delta T/T$. The long delay ($>$4 ns) between the pump and white light pulses was controlled using an electronic delay generator (Stanford Research Systems

DG535). For short pump–probe delay times smaller than 4 ns, the chopped optical output of a collinear optical parametric amplifier with a second harmonic generator (Light Conversion Orpheus, Lyra) was used. The pump–probe delay is adjusted using a linear translation stage (Thorlabs DDS600/M).

Results and discussion

In all donor–acceptor dyads (BPDs), examined in this work, BODIPY plays the role of an electron acceptor and pyrene acts as an electron donor (Fig. 1c), providing ultrafast electron transfer from pyrene to the BODIPY subunit. To achieve an effective PET, the donor subunit is attached directly in the meso-position of the BODIPY which results in orthogonal geometry (dihedral angles of 81°–89°). The formation of triplet states in these dyads *via* SOCT-ISC can take place in solvents of different polarity (from non-polar hexane to strongly polar acetonitrile).[63] Recently, the efficiency of triplet state generation in these dyads was investigated by measuring the singlet oxygen quantum yield (Φ_Δ).[62] Dyad BPD1 displayed the highest Φ_Δ value of 0.75 in ethanol, whereas dyads BPD2 and BPD3 displayed lower Φ_Δ values (0.25–0.34). Dyad BPD4 bearing six alkyl groups showed a much lower Φ_Δ value of 0.04. This trend can be explained by a decrease in the driving force of PET with an increase in the number of alkyl groups. Buck *et al.* demonstrated that the presence of four methyl groups in the BODIPY core makes electron transfer in BPD3 thermodynamically unfavourable even in very polar acetonitrile (ΔG_{PET} = 0.083 eV). The presence of two

additional ethyl groups in BPD4 further reduces the driving force of the process (ΔG_{PET} = 0.27 eV).[58]

Since perylene, which was employed in this work as the TTA-UC emitter, is poorly soluble in highly polar solvents (ethanol and acetonitrile), we performed spectroscopic characterization of dyads in less polar solvents like DCM and THF.

Optical characterization of BPDs

The UV-Vis absorption (Fig. 2a and b) and emission (Fig. 2c and d) spectra of BPDs in DCM and THF are presented in Fig. 2. The absorption spectra of all dyads exhibit a pyrene band at around 300–400 nm and a BODIPY band at around 450–550 nm for all four BPD molecules. For BPD1 and BPD3, the BODIPY band lies around 505 nm, whereas BPD4 shows a red-shifted band at around 528 nm. The position of the absorption peak of BPD2 (with the maximum at 515 nm) is intermediate between BPD1 and BPD4. The absorption maxima are independent of solvent polarity. However, the polarity has a strong effect on the emission spectra as it is presented in Fig. 2c and d.

BPD1 demonstrates a strongly red-shifted emission band compared to regular BODIPYs. The emission is centred at 680 nm in THF and 700 nm in DCM. This emission originates from the CT state and exhibits moderate ϕ_F values of 8.0% and 7.0%,[31] with decay times of 4 ns and 3.3 ns in THF and DCM (see Fig. S1a and S2a, ESI†), respectively. Although CT states are generally considered to be dark, recent results have indicated enhanced emissivity of CT states in dyads based on the alkyl-unsubstituted BODIPY scaffold, proposed to be caused by
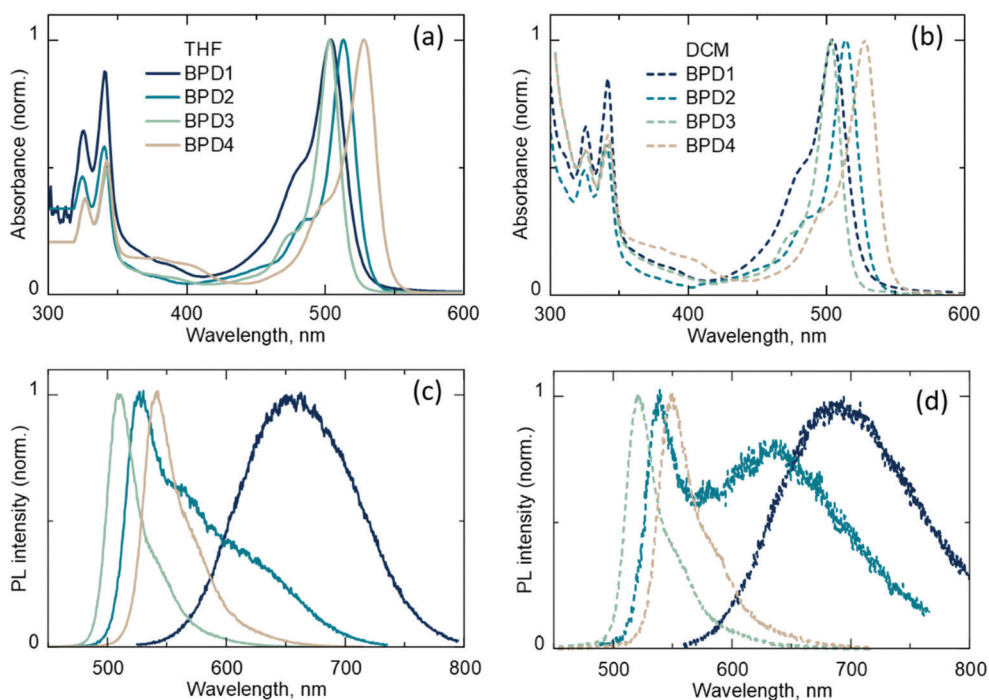

Fig. 2 (a) Normalized UV-Vis absorption spectra of BPDs in tetrahydrofuran (THF); (b) normalized UV-Vis absorption spectra of BPDs in dichloromethane (DCM); (c) normalized emission spectra of BPDs in THF (excitation – 355 nm); (d) normalized emission spectra of BPDs in DCM (excitation – 355 nm).

increased electronic coupling between the electron donor and acceptor subunits.[64]

The dyad with two methyl groups (BPD2) in DCM displays an emission peak around 540 nm, which corresponds to the radiative transition $S_1 \rightarrow S_0$ and an additional red-shifted shoulder peak at around 640 nm, which corresponds to the emission of the CT state ($^1CT \rightarrow S_0$). The transitions have a similar decay time of 4.6 ns in DCM and slightly different decay times of 7.4 ns and 6.6 ns in THF solvent (Fig. S2b, ESI†), respectively. In contrast to alkyl-unsubstituted and dialkyl-substituted BODIPY scaffolds, BPD3 and BPD4 dyads with four and six alkyl groups display typical BODIPY emission spectra for both solvents with peaks in the region of 500–550 nm and decay times of 5.6 ns and 6.7 ns in DCM, and 10.2 ns and 11.2 ns in THF, respectively. Thus, it can be assumed that BPD3 and BPD4 do not undergo PET in solvents with moderate polarity (DCM and THF) as opposed to BPD1 and BPD2, or their charge-transfer states (^1CT) are not emissive.

The decay times of the charge-transfer emission for dyads BPD1 and BPD2, which are in the range of 3–6.6 ns, shed light on the kinetics of the intersystem crossing. It can be assumed that ISC in these molecules is a relatively slow process with a rate constant in the range of ns^{-1}. ISC in these systems can in principle lead to the formation of two different triplet states: charge transfer (T_{CT}) and local triplet (T_{BODIPY}) states formed by radical-pair ISC (RP-ISC) and SOCT-ISC, respectively, whereas a

second local triplet state (T_{Pyr}) is unlikely to be attainable due to its high energy of 2.09 eV.[65] It should be noted that the formation of the T_{CT} state via RP-ISC is also quite debatable, since recently Buck et al. have provided experimental evidence for the absence of RP-ISC in similar electron-donor–acceptor dyads.[58] It is known that BODIPY triplet states are poorly emissive; however, the corresponding phosphorescence can be detected in a glassy solvent matrix at low temperatures.[66] Therefore, the PL spectra of the BPDs dissolved in ethanol at low temperatures (down to 40 K) were investigated in detail. It was expected that highly polar ethanol can additionally facilitate the formation of triplet states and provide a good glassy matrix for detection of the triplet emission.

Fig. 3a demonstrates the PL spectra of BPD1 at different temperatures. At less than 140 K, the appearance of a new peak in the near-infrared (NIR) range was observed, with a maximum of 735 nm (1.69 eV).

The decay time of the peak exceeds the 1 ms time window of the streak camera, and it is therefore concluded that these must be long-lived triplet states formed by SOCT-ISC. It should be pointed out that the triplet energy of the BODIPY molecule reported in the literature (1.7 eV)[66] is close to the 735 nm peak and, thus, this triplet level can be assigned to the T_{BODIPY} state. The low temperature PL spectrum of the BPD2 dyad reveals a NIR peak with a maximum of 765 nm (1.62 eV), which probably also belongs to the T_{BODIPY} state. Low-temperature PL measurements for dyads BPD3 and BPD4 (Fig. 3c and d) do not display any
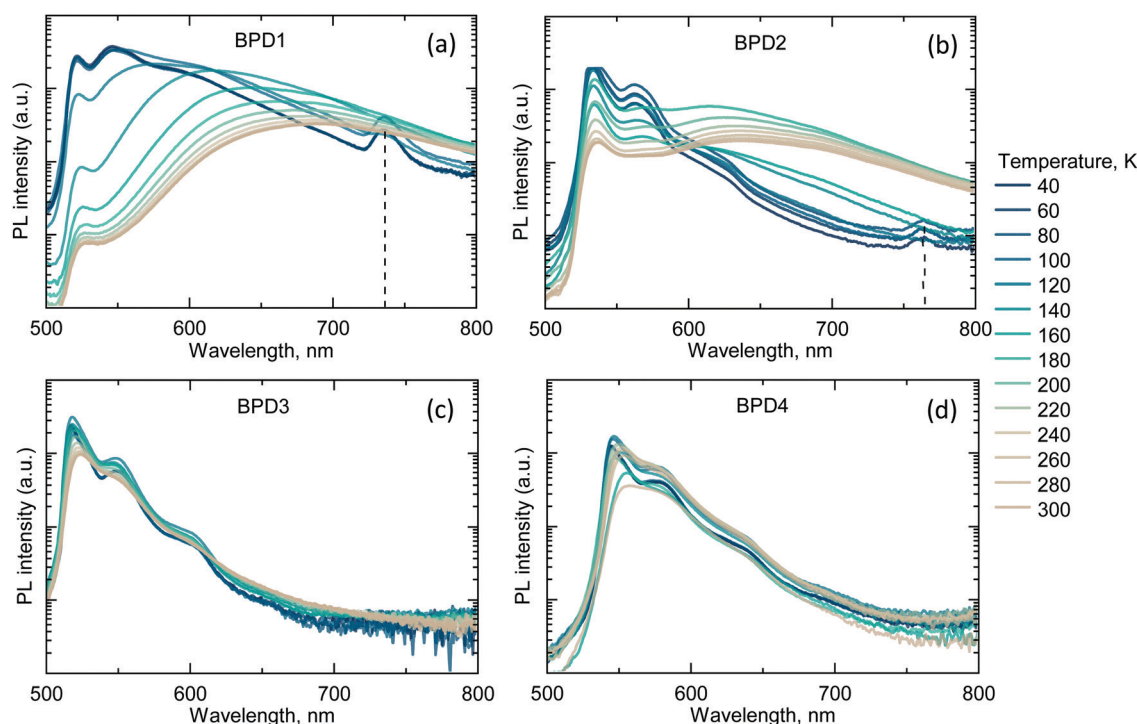
Fig. 3 (a) Emission spectra of BPD1 at different temperatures (excitation – 405 nm). Emission of the S_{CT} state demonstrates a hypsochromic shift with the temperature decrease. Furthermore, emissions of S_1 and S_{CT} states are observable alongside the characteristic longer wavelength T_{BODIPY} phosphorescence (735 nm) at temperatures < 140 K (in supercooled solvent glass); (b) emission spectra of BPD2 at different temperatures. BPD2 emission spectra show similar temperature dependence to those of BPD1; (c) and (d) emission spectra of BPD3 and BPD4, respectively, measured at different temperatures. Emissions of BPD3 and BPD4 do not display any additional NIR peaks at low temperatures.

additional peaks and, therefore, it can be concluded that these molecules possess inefficient ISC.

TTA-UC with BPDs used as sensitizers

Using variable-temperature PL measurements, triplet states with energies of >1.62 eV were detected for BPD1 and BPD2 dyads. Therefore, these dyads can be paired with perylene (with a lower triplet energy of 1.53 eV) to realize TTA-UC. Indeed, the BPD1 dyad mixed with perylene in solvents with moderate polarity (deoxygenated THF and DCM) demonstrated bright UC luminescence with characteristic features of perylene luminescence (420–500 nm) and broad luminescence from the CT state (550–900 nm) (Fig. 4a). The BPD2 dyad paired with perylene also demonstrated strong UC PL in DCM, whereas the THF solution only exhibited strong luminescence of BPD2 and only an extremely weak UC signal (Fig. 5a). To quantify TTA-UC intensity, measurements of ϕ_{UC} were performed using a relative method.[31] The calculated ϕ_{UC} values are presented in Table 1. The highest ϕ_{UC} value of 6.9% was observed for the BPD1 dyad in THF solution. The same dyad in DCM demonstrates a lower ϕ_{UC} value of 2.5%. The opposite trend was found for BPD2, where the highest ϕ_{UC} of 4.7% was measured in DCM and only extremely weak UC luminescence is observed in THF. It should be noted that no UC luminescence was detected for dyads BPD3 and BPD4 in either DCM or THF.

To shed light on TTA-UC with heavy-atom-free sensitizers, the efficiency of each individual step (as illustrated earlier in

eqn 1) was investigated. Efficiencies of intersystem crossing (ϕ_{ISC}) for BPD1 and BPD2 dyads were assessed using TA spectroscopy. As depicted in Fig. 4b and 5b, we were able to measure the time evolution of the ground-state bleaching with short (ps–ns) and long (ns–μs) delays using the same setup and the same excitation settings. It was assumed that ground state bleaching is the dominant signal at 505 nm and 515 nm (for BPD1 and BPD2, respectively), while the other signals attributed to excited state absorption are much less prominent at these wavelengths. Therefore, after normalization of the TA transients, the amplitude value of the long component (in the μs range) should be proportional to the efficiency of ISC:

$$\phi_{ISC} \approx A \times 100\%, \qquad (3)$$

where A is the amplitude of the long-lived component of the decays as depicted in both Fig. 4b and 5b.

The estimated ϕ_{ISC} values are presented in Table 1. The highest value of ϕ_{ISC} of 58% was observed for BPD1 in THF. A similar value of 56% was calculated for BPD2 in DCM, while BPD1 exhibited a slightly lower value of $\phi_{ISC} = 49\%$ in this solvent. It can be assumed that the parameter ϕ_{ISC} is independent of both intensity and concentration, and therefore the obtained values can be directly used in eqn (1).

Measurements of TA with long delay (ns–μs) also assist in estimating TTET efficiency from the triplet state of dyads to the perylene triplet state. For instance, Fig. S3–S5 (ESI†) demonstrate
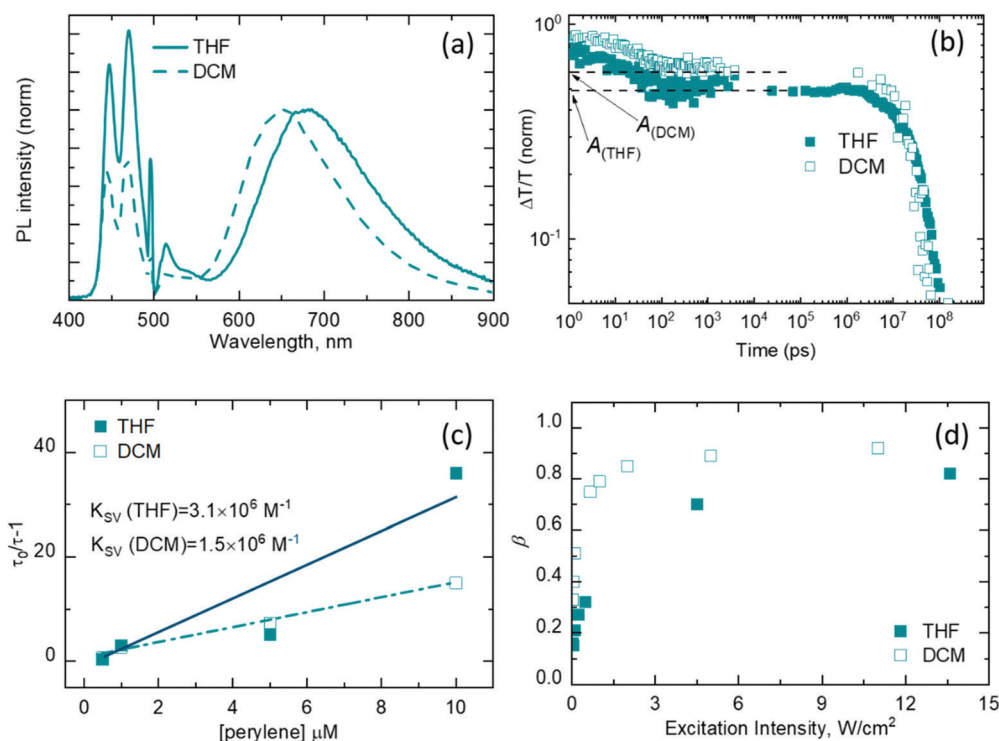
Fig. 4 (a) Normalized UC luminescence of the BPD1–perylene mixture (1 : 10 molar ratio) under 498 nm excitation (power density of 5 W cm^{-2}) (C_{BPD1} = 1 × 10^{-5} M) in deoxygenated THF (blue solid line) and DCM (dashed blue line); (b) transients (measured at 505 nm) from TA experiments for the BPD1–perylene mixtures in deoxygenated THF and DCM. Dashed lines indicate the value of A used in the estimation of ϕ_{ISC}; (c) Stern–Volmer plots for BPD1–perylene (C_{BPD1} = 1 × 10^{-4} M) in deoxygenated THF and DCM. (d) Efficiency of triplet–triplet annihilation as a function of excitation intensity for BPD1–perylene mixtures in deoxygenated THF and DCM.
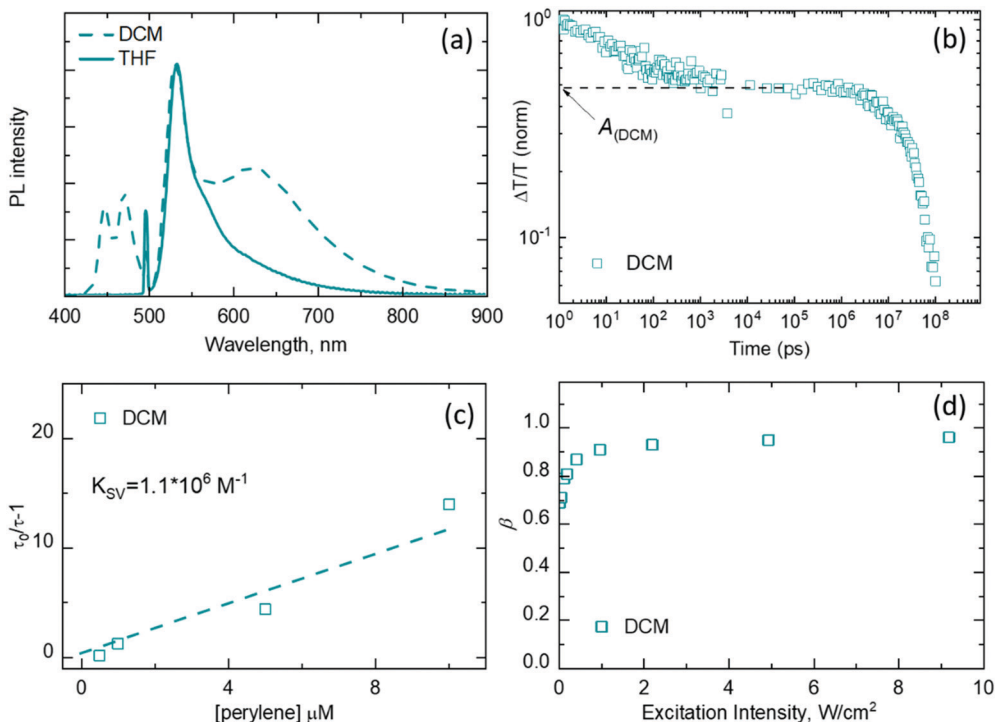
Fig. 5 (a) UC luminescence of the BPD2–perylene mixture (1 : 10 molar ratio) under 498 nm excitation (power density of 5 W cm^{-2}) (C_{BPD2} = 1 × 10^{-5} M) in deoxygenated THF (blue solid line) and DCM (dashed blue line). (b) Transients (measured at 515 nm) from TA experiments for the BPD2–perylene mixture in deoxygenated DCM. Dashed lines indicate the value of A used in the estimation of ϕ_{ISC}. (c) Stern–Volmer plots for BPD2–perylene (C_{BPD2}= 1 × 10^{-4} M) in deoxygenated DCM. (d) Efficiency of triplet–triplet annihilation as a function of excitation intensity for BPD2–perylene mixtures in deoxygenated DCM.

Table 1 Overall quantum yield and efficiencies of the individual steps of the TTA-UC process for BPD1 (in DCM and THF) and BPD2 (in DCM)

	BPD1 (DCM)	BPD1 (THF)	BPD2 (DCM)
ϕ_{UC},[a] %	2.5	6.9	4.7
ϕ_{ISC},[b] %	49	58	56
ϕ_{TTET},[c] %	99	99	99
ϕ_{TTA},[d] %	92	83	94
ϕ_{F},[e] %	71	85	71
f_{TTA}[f]	0.15	0.33	0.25

[a] Measured at an intensity of 5 W cm^{-2} (498 nm laser) using eqn (2) for BPD and perylene concentrations of 10^{-5} M and 10^{-4} M, respectively. [b] Estimated for a BPD concentration of 10^{-5} M. [c] Estimated using eqn (5) for BPD and perylene concentrations of 10^{-5} M and 10^{-4} M, respectively. [d] Estimated using eqn (6) with BPD and perylene concentrations of 10^{-5} M and 10^{-4} M, respectively. The reported values correspond to intensities (525 nm laser) of 12 W cm^{-2} and 3.6 W cm^{-2} for BPD1 and BPD2, respectively. [e] Estimated using an integrating sphere for a perylene concentration of 10^{-4} M. [f] Calculated using eqn (1).

the TA spectra for pure BPD1 and BPD2, as well as for BPD1–perylene and BPD2–perylene mixtures. In these results, transients of the ground state bleach (505 nm and 515 nm for BPD1 and BPD2, respectively) follow the mono-exponential kinetics and their decay times are equal to the decay time of the triplet state (T$_{BODIPY}$). Thus, the values of 37 μs, 37 μs, and 44 μs were obtained for BPD1 in DCM, BPD1 in THF and BPD2 in DCM, respectively. The τ_0 values for BPD1 are consistent with earlier measurements performed in DMF, where a value of 36 μs was reported.[62]

A series of measurements of triplet state lifetime at different concentrations of the triplet quencher (perylene) allow assessment of the Stern–Volmer constant (K_{SV}) using the equation:

$$\tau_0/\tau = 1 + K_{SV} \text{[perylene]}, \qquad (4)$$

where τ_0 and τ are the lifetimes of the dyad triplet state without and with the quencher and [perylene] is the molar concentration of perylene.

Stern–Volmer plots for the BPD1 dyad measured in DCM and THF are presented in Fig. 4c. The linear fit of the data results in Stern–Volmer constants of K_{SV} = 3.1 × 10^6 M^{-1} in THF and K_{SV} = 1.5 × 10^6 M^{-1} in DCM. These values of K_{SV} are in line with the earlier found K$_{SV}$ constants for quenching of BODIPY–phenoxazine dyads by perylene (1.06 × 10^6 M^{-1} and 1.59 × 10^6 M^{-1}).[53] The values of τ_0 allow us to additionally calculate the quenching constant $k_q = K_{SV}/\tau_0$, which leads to the values of k_q = 8.4 × 10^{10} M^{-1} s^{-1} and k_q = 4.1 × 10^{10} M^{-1} s^{-1}. These values, in turn, are very close to diffusion-controlled bimolecular quenching rate constants of ~10^{10}–10^{11} M^{-1} s^{-1} (calculated for BODIPY–phenoxazine dyads in toluene and hexane, respectively).[53] The obtained K_{SV} values ensure that, at an emitter concentration of 10^{-5} M, perylene almost completely quenches the triplet states of BPD1 with efficiencies of 93.7% and 97.2% (eqn (5)) in DCM and THF, respectively.

$$\phi_q = \phi_{TTET} = (1 - \tau/\tau_0) \times 100\%, \qquad (5)$$

Using the K_{SV} values and eqn (5), it was also possible to calculate the values of ϕ_{TTET} for the typical concentration of the emitter in our UC experiments of 10^{-4} M. Under these conditions, ϕ_{TTET} approaches 99% for BPD1 solutions in both DCM and THF. Quenching of the BPD2 dyad by perylene is also very effective in DCM with $K_{SV} = 1.1 \times 10^6$ M^{-1} (Fig. 5c), $k_q = 2.5 \times 10^{10}$ M^{-1} s^{-1}, and $\phi_{TTET} = 99\%$ (for a perylene concentration of 10^{-4} M).

To estimate ϕ_{TTA}, UC decays at different excitation intensities were measured. These decays measured in the intensity range of 0.03–15 W cm^{-2} are plotted in Fig. S6–S8 (ESI†). According to the method proposed by Cheng et al.,[67] the global fitting of these decays using eqn (6) enables determining the parameters k_{EM} and β:

$$I_{UC}(t) \propto I_{UC}(0) \left(\frac{1 - \beta}{\exp(k_{EM}t) - \beta} \right)^2, \qquad (6)$$

where $I_{UC}(t)$ is the intensity of UC and $I_{UC}(0)$ at time t is the UC intensity at time = 0 ($I_{UC}(0) = 1$ for a normalized decay), k_{EM} represents the decay rate of the triplet state and β is defined as the initial fraction of triplets decaying via bimolecular TTA from all decaying processes.

This method was originally developed for a pulsed excitation (with a short fs-pulse) where $\phi_{TTA} < \beta$. However, for the method used in our work (with cw-laser modulated with a frequency of 100 Hz and a duty cycle of 50%, see the experimental part for details) the β value obtained with eqn (6) can be converted to ϕ_{TTA} using a simple approximation $\phi_{TTA} \approx \beta$.

It is necessary to note that that ϕ_{UC} values were measured using 498 nm excitation (close to the absorption maximum of BPD sensitizers). However, this laser cannot be modulated to measure UC transients. Therefore, a laser diode with a wavelength of 525 nm was used to measure UC lifetimes. Given the difference in absorption at 498 and 525 nm, the correction factor should be introduced for comparison of ϕ_{UC} and ϕ_{TTA}. Assuming an equal flux of absorbed photons, ϕ_{UC} measured at 5 W cm^{-2} of a 498 nm laser corresponds to ϕ_{TTA} measured at 12 W cm^{-2} for BPD1 in DCM and THF, as well as at 3.6 W cm^{-2} for BPD2 in DCM. Fig. 4d displays the rise of $\beta = \phi_{TTA}$ up to 92% (at 12 W cm^{-2}) in DCM and up to 83% (at 12 W cm^{-2}) in THF. Furthermore, global fitting of the data obtained for the BPD1–perylene mixtures in DCM (Fig. S6, ESI†) and THF (Fig. S7, ESI†) gives k_{EM} values of 0.78 ms^{-1} and 1.59 ms^{-1}, respectively. This corresponds to the lifetimes of the perylene triplet state of $\tau_{perylene}^T = 1/k_{EM} = 1.3$ ms and 0.65 ms, respectively. Global fitting of UC decays for the BPD2–perylene mixture in DCM (Fig. S8, ESI†) results in $\tau_{perylene}^T = 1.1$ ms and the intensity dependence of β (Fig. 5d) which gives $\phi_{TTA} = 94\%$ (at 3.6 W cm^{-2}).

To estimate further the yield of singlet states generated via the TTA process, ϕ_{TTA} needs to be multiplied by the statistical factor f_{TTA}, which considers spin statistics of TTA.[67] The TTA is usually assumed to occur through the formation of a complex between the two emitters in their triplet states. The complexes can have different multiplicity, and the probability of forming complexes with a certain multiplicity (singlet, triplet, or quintet) should correspond to the ratio of $1:3:5$, respectively. This statistic predicts $f_{TTA} = 0.11$, if TTA occurs via complexes with all possible multiplicity; $f_{TTA} = 0.4$, if TTA occurs via complexes with singlet and triplet multiplicity; and $f_{TTA} = 1$, if only the complex with singlet multiplicity is involved in the TTA process.

The rise and saturation of β have a strong relationship to a figure-of-merit UC parameter – UC threshold (I_{th}). At intensities far greater than I_{th}, bimolecular TTA dominates over monomolecular decays and ϕ_{TTA} approaches a constant value. The I_{th} value can be roughly estimated by approximating the dependency of UC intensity vs. excitation intensity ($\ln(I_{UC}) \propto \ln(P_{exc})$) by two straight lines (for low and high excitation intensities) and finding their intersection point. However, it is not always possible to investigate UC in a very broad excitation intensity range to identify quadratic (with slope $n = 2$) and linear (with slope $n = 1$) regimes. For instance, Fig. S9a (ESI†) illustrates the UC behaviour of the BPD1/perylene pair measured in DCM using various excitation intensities. The slope gradually changes from $n = 1.5$ (at 0.1 W cm^{-2}) down to $n = 1.15$ (at 8 W cm^{-2}), which makes the I_{th} estimate rather arbitrary. On the other side, a ratio of UC intensity to excitation intensity (I_{UC}/I) changes proportionally to ϕ_{UC} (Fig. S9b, ESI†). We assumed that the values of $\phi_{UC} > 0.5 \times \phi_{UC}^{max}$ can be relevant for practical applications.[68] Thus, the value of excitation intensity corresponding to $\phi_{UC} \approx 0.5 \times \phi_{UC}^{max}$ was used as I_{th} and the values of 0.3 W cm^{-2} and 0.03 W cm^{-2} were estimated for BPD1 (Fig. S9b, ESI†) and BPD2 (Fig. S10b, ESI†) in DCM, respectively.

To complete measurements of the parameters included in eqn (1), the photoluminescence quantum yields (ϕ_F) of perylene in THF and DCM were measured using the absolute method in an integrating sphere resulting in values of $\phi_F = 71\%$ in DCM and $\phi_F = 85\%$ in THF.

Comparison of BPDs as sensitizers for TTA-UC

It has been previously demonstrated that BPDs bearing tetra- and hexa-substituted BODIPY scaffolds are not able to efficiently generate singlet oxygen.[62] The results from this work agree with this in that neither BPD3 nor BPD4 dyads are not able to sensitize TTA-UC in THF or DCM. More polar solvents (ethanol or acetonitrile) were not investigated here due to the limited solubility of perylene in these solvents. The lack of TTA-UC with BPD3 and BPD4 sensitizers can be explained by the very limited ISC in these molecules due to thermodynamically unfavoured PET.[58] Unlike BPD3 and BPD4, the dyad with two alkyl groups (BPD2) and the unsubstituted dyad (BPD1) exhibit sensitization of TTA-UC in DCM, while only the BPD1 dyad demonstrates efficient UC in THF.

Comparing the results (Table 1) obtained for the BPD1 dyad in DCM and THF provides several important observations. The UC sensitized with the BPD1 dyad demonstrates comparable values of ϕ_{TTA} and ϕ_{TTET} in both solvents. Therefore, at first glance, the rather significant difference in ϕ_{UC} (2.5% in DCM vs. 6.9% in THF) can be explained by the differences in ϕ_{ISC} and ϕ_F.

However, accounting for the rather small difference in these parameters our attention was focused on the values of f_{TTA}.

It has previously been demonstrated that for UC with the highest quantum yield the perylene dimer (ϕ_{UC} = 42%, emitter concentration of 5×10^{-4} M) and perylene (ϕ_{UC} = 38%, emitter concentration of 1×10^{-4} M) sensitized by Pd(II)- and Pt(II)-tetrabenzoporphyrin complexes in THF exhibit values of f_{TTA} = 1 and saturated ϕ_{TTA} close to 100%.[27,69] In our work we extracted f_{TTA} = 0.33 (using eqn (1) and the results presented in Table 1) for UC in THF with the concentration of BPD1 and perylene (10^{-5} M and 10^{-4} M, respectively). On the other side, Wei et al.[70] reported $0.11 < f_{TTA} < 0.4$ for perylene paired with the BODIPY-phenyl-C$_{60}$ dyad in THF (perylene concentration of 4.5×10^{-3} M). Thus, the literature reports quite different values for f_{TTA} even for the same solvent (THF), while our result of f_{TTA} = 0.32 is closer to the results reported by Wei et al.[69] Furthermore, the f_{TTA} values of 0.15 and 0.25 were obtained for UC sensitized with BPD1 and BPD2 in DCM, respectively. Several recent papers have discussed a number of reasons explaining additional loss channels in TTA-UC, which may manifest as a false reduction in f_{TTA}.[71-73] For example, it was noticed that singlet and triplet energy landscapes can change in a conformationally flexible emitter (9,10-bis(phenylethynyl)anthracene) and the energetic requirement $2 \times E_{T1} > E_{S1}$ for efficient TTA-UC is not fulfilled for all rotational conformers.[71] In addition, in the case of the perylene emitter, triplet excimer formation in solution may also change the triplet and singlet state energies, which may lead to less efficient UC and is reflected in the apparent change of f_{TTA} in different solvents and at different emitter concentrations.[72] However, the perylene used as the emitter in this study shows no evidence of excimer formation (observed as a sharp fluorescence peak with a maximum at 565 nm[73]). Thus, the observed discrepancies in the f_{TTA} values for perylene cannot be still explained unambiguously.

Importantly, the high values of ϕ_{TTA} found for BPD2 in DCM are evident in the low I_{th} (Fig. S9 and S10, ESI†). However, the value of $I_{th} \sim$ 30 mW cm^{-2} is still high to be considered useful for applications requiring an intensity of 1 Sun equivalent ($\sim$3–5 mW cm^{-2}). Both I_{th} and ϕ_{UC} can be further improved by tuning the chemical structure of the sensitizer and emitter, as well as finding the best solvent and optimizing the sensitizer and emitter concentrations.

The BPD1 and BPD2 sensitizers in THF and DCM demonstrate $\phi_{ISC} \approx$ 0.5 which is significantly lower than $\phi_{ISC} \approx$ 1 for benchmark photosensitizer–porphyrin complexes of noble metals (Pd(II) or Pt(II)). We assume that the efficiency of intersystem crossing for the investigated sensitizers can be improved by finding an optimal solvent to enhance formation of the CT state and SOCT-ISC. For example, the luminescence of the BPD1 CT state in DCM and THF is an important deactivation channel that competes with relatively slow SOCT-ISC. This luminescence is significantly reduced in the polar solvent (DMF)[62] which indicates an increase of SOCT-ISC efficiency.

However, even more attention should be paid to the choice of the emitter, as perylene is insoluble in polar solvents and demonstrates in our experiments very low f_{TTA} values (in the range of 0.15–0.32). Recently, Bossanyi et al.[74] demonstrated that f_{TTA} can vary from 0.4 to 1 depending on the orientation of molecules in the triplet dimers (TT), the energy gap between E$_{(TT)}$ and E$_{T2}$, as well as the reverse intersystem crossing T$_2 \rightarrow$ S$_1$. Thus, a fine modification of the chemical structure of perylene could probably improve its solubility and enable an increase in f_{TTA} and the rate of TTA, increasing ϕ_{UC} in general.

Conclusions

In this work we investigated the photosensitization of TTA-UC using heavy-atom-free donor–acceptor BODIPY–pyrene dyads (BPDs) paired with perylene as the emitter. Dyads with four and six alkyl substituents in the BODIPY scaffold (BPD3 and BPD4) are not capable of producing UC luminescence, whereas dyads with two methyl groups and an unsubstituted BODIPY scaffold (BPD1 and BPD2) exhibit UC with quantum efficiencies up to 6.9% (at 498 nm laser excitation intensity of 5 W cm^{-2}) and a low UC threshold (down to $\sim$ 30 mW cm^{-2}). This efficient UC was explained through evaluation of elementary step efficiencies contributing to the ϕ_{UC} integral value. The BPD1 and BPD2 dyads demonstrate SOCT-ISC in moderate polarity solvents (THF and DCM) with efficiencies of 49–58%. We found that SOCT-ICS populates BODIPY triplet states with energies of 1.69 and 1.62 eV for BPD1 and BPD2, respectively. Furthermore, both dyads allow energy transfer to perylene triplet states at transfer rates (quenching constants in the range of 2.2–8.8 $\times$ 10^{10} M^{-1} s^{-1}) close to the diffusion limit. The TTA efficiency values estimated from UC transitions measured at different intensities are high (up to 94% at an excitation (488 nm) intensity of 5 W cm^{-2}) and these measurements confirm a spin statistical factor (f_{TTA}) close to 0.4. Thus, ISC (with efficiency of $\sim$50%) and the poor statistics of the TTA step currently limit the effectiveness of TTA-UC. We hope to overcome these limitations in the future by finding better solvents as well as emitters with higher f_{TTA}.

Author contributions

The manuscript was written through the contributions of all authors. N. K., J. C. F., M. K., M. J. and D. B. conducted spectroscopic experiments and N. K. wrote the paper. M. F. synthesized the BPD molecules. B. S. R. and A. T. developed the original concept of the paper. A. T., I. A. H. and B. S. R. contributed equally to scoping and structuring the paper and provided additional guidance on experimental methods. All authors have approved the final version of the manuscript.

Conflicts of interest

There are no conflicts to declare.

Acknowledgements

References

1 C. Wohnhaas, A. Turshatov, V. Mailänder, S. Lorenz, S. Baluschev, T. Miteva and K. Landfester, *Macromol. Biosci.*, 2011, **11**, 772–778.

2 Q. Liu, T. Yang, W. Feng and F. Li, *J. Am. Chem. Soc.*, 2012, **134**, 5390–5397.

3 S. H. C. Askes, M. S. Meijer, T. Bouwens, I. Landman and S. Bonnet, *Molecules*, 2016, **21**, 1460.

4 Q. Liu, M. Xu, T. Yang, B. Tian, X. Zhang and F. Li, *ACS Appl. Mater. Interfaces*, 2018, **10**, 9883–9888..

5 H.-L. Lee, J. H. Park, H.-S. Choe, M.-S. Lee, J.-M. Park, N. Harada, Y. Sasaki, N. Yanai, N. Kimizuka, J. Zhu, S. H. Bhang and J.-H. Kim, *ACS Appl. Mater. Interfaces*, 2019, **11**, 26571–26580.

6 T. F. Schulze and T. W. Schmidt, *Energy Environ. Sci.*, 2015, **8**, 103–125.

7 L. Frazer, J. K. Gallaher and T. W. Schmidt, *ACS Energy Lett.*, 2017, **2**, 1346–1354.

8 T. Dilbeck and K. Hanson, *J. Phys. Chem. Lett.*, 2018, **9**, 5810–5821.

9 Y. Zhou, C. Ruchlin, A. J. Robb and K. Hanson, *ACS Energy Lett.*, 2019, **4**, 1458–1463.

10 J.-H. Kim and J.-H. Kim, *J. Am. Chem. Soc.*, 2012, **134**, 17478–17481.

11 H.-i. Kim, O. S. Kwon, S. Kim, W. Choi and J.-H. Kim, *Energy Environ. Sci.*, 2016, **9**, 1063–1073..

12 O. S. Kwon, J.-H. Kim, J. K. Cho and J.-H. Kim, *ACS Appl. Mater. Interfaces*, 2015, **7**, 318–325.

13 B. Pfund, D. M. Steffen, M. R. Schreier, M.-S. Bertrams, C. Ye, K. Börjesson, O. S. Wenger and C. Kerzig, *J. Am. Chem. Soc.*, 2020, **142**, 10468–10476.

14 J. Isokuortti, K. Kuntze, M. Virkki, Z. Ahmed, E. Vuorimaa-Laukkanen, M. A. Filatov, A. Turshatov, T. Laaksonen, A. Priimagi and N. A. Durandin, *Chem. Sci.*, 2021, **12**, 7504–7509.

15 M. Barawi, F. Fresno, R. Pérez-Ruiz and V. A. de la Peña O'Shea, *ACS Appl. Energy Mater.*, 2019, **2**, 207–211.

16 A. L. Hagstrom, H.-L. Lee, M.-S. Lee, H.-S. Choe, J. Jung, B.-G. Park, W.-S. Han, J.-S. Ko, J.-H. Kim and J.-H. Kim, *ACS Appl. Mater. Interfaces*, 2018, **10**, 8985–8992.

17 S. Wen, J. Zhou, P. J. Schuck, Y. D. Suh, T. W. Schmidt and D. Jin, *Nat. Photonics*, 2019, **13**, 828–838.

18 J. Pedrini and A. Monguzzi, *J. Photonics Energy*, 2017, **8**, 022005.

19 M. Oldenburg, A. Turshatov, D. Busko, S. Wollgarten, M. Adams, N. Baroni, A. Welle, E. Redel, C. Wöll, B. S. Richards and I. A. Howard, *Adv. Mater.*, 2016, **28**, 8477–8482.

20 F. Meinardi, M. Ballabio, N. Yanai, N. Kimizuka, A. Bianchi, M. Mauri, R. Simonutti, A. Ronchi, M. Campione and A. Monguzzi, *Nano Lett.*, 2019, **19**, 2169–2177.

21 E. Radiunas, S. Raišys, S. Jurėnas, A. Jozeliūnaitė, T. Javorskis, U. inkevičiūtė, E. Orentas and K. Kazlauskas, *J. Mater. Chem. C*, 2020, **8**, 5525–5534.

22 M. Wu, T.-A. Lin, J. O. Tiepelt, V. Bulović and M. A. Baldo, *Nano Lett.*, 2021, **21**, 1011–1016.

23 J. Zhou, Q. Liu, W. Feng, Y. Sun and F. Li, *Chem. Rev.*, 2015, **115**, 395–465.

24 W. Zou, C. Visser, J. A. Maduro, M. S. Pshenichnikov and J. C. Hummelen, *Nat. Photonics*, 2012, **6**, 560–564.

25 J. Zhao, W. Wu, J. Sun and S. Guo, *Chem. Soc. Rev.*, 2013, **42**, 5323–5351.

26 D. Dzebo, K. Moth-Poulsen and B. Albinsson, *Photochem. Photobiol. Sci.*, 2017, **16**, 1327–1334.

27 S. Hoseinkhani, R. Tubino, F. Meinardi and A. Monguzzi, *Phys. Chem. Chem. Phys.*, 2015, **17**, 4020–4024.

28 Y. Y. Cheng, T. Khoury, R. G. C. R. Clady, M. J. Y. Tayebjee, N. J. Ekins-Daukes, M. J. Crossley and T. W. Schmidt, *Phys. Chem. Chem. Phys.*, 2010, **12**, 66–71.

29 N. Yanai, K. Suzuki, T. Ogawa, Y. Sasaki, N. Harada and N. Kimizuka, *J. Phys. Chem. A*, 2019, **123**, 10197–10203.

30 Y. Zhou, F. N. Castellano, T. W. Schmidt and K. Hanson, *ACS Energy Lett.*, 2020, **5**, 2322–2326.

31 N. Kiseleva, D. Busko, B. S. Richards, M. A. Filatov and A. Turshatov, *J. Phys. Chem. Lett.*, 2020, **11**, 6560–6566.

32 T. Yogo, Y. Urano, Y. Ishitsuka, F. Maniwa and T. Nagano, *J. Am. Chem. Soc.*, 2005, **127**, 12162–12163.

33 K. Chen, Y. Dong, X. Zhao, M. Imran, G. Tang, J. Zhao and Q. Liu, *Front. Chem.*, 2019, **7**, 821.

34 K. N. Solov'ev and E. A. Borisevich, *Phys.-Usp.*, 2005, **48**, 231–253.

35 V. Gray, P. Xia, Z. Huang, E. Moses, A. Fast, D. A. Fishman, V. I. Vullev, M. Abrahamsson, K. Moth-Poulsen and M. Lee Tang, *Chem. Sci.*, 2017, **8**, 5488–5496.

36 L. Nienhaus, M. Wu, N. Geva, J. J. Shepherd, M. W. B. Wilson, V. Bulović, T. Van Voorhis, M. A. Baldo and M. G. Bawendi, *ACS Nano*, 2017, **11**, 7848–7857.

37 M. Mahboub, Z. Huang and M. L. Tang, *Nano Lett.*, 2016, **16**, 7169–7175.

38 N. Nishimura, J. R. Allardice, J. Xiao, Q. Gu, V. Gray and A. Rao, *Chem. Sci.*, 2019, **10**, 4750–4760.

39 E. M. Gholizadeh, S. K. K. Prasad, Z. L. Teh, T. Ishwara, S. Norman, A. J. Petty, J. H. Cole, S. Cheong, R. D. Tilley, J. E. Anthony, S. Huang and T. W. Schmidt, *Nat. Photonics*, 2020, **14**, 585–590.

40 Z. A. VanOrman, C. R. Conti, G. F. Strouse and L. Nienhaus, *Chem. Mater.*, 2021, **33**, 452–458.

41 K. Mase, K. Okumura, N. Yanai and N. Kimizuka, *Chem. Commun.*, 2017, **53**, 8261–8264.

42 S. He, X. Luo, X. Liu, Y. Li and K. Wu, *J. Phys. Chem. Lett.*, 2019, **10**, 5036–5040.

43 K. Okumura, N. Yanai and N. Kimizuka, *Chem. Lett.*, 2019, **48**, 1347–1350.

44 S. He, R. Lai, Q. Jiang, Y. Han, X. Luo, Y. Tian, X. Liu and K. Wu, *Angew. Chem., Int. Ed.*, 2020, **59**, 17726–17731.

45 Z. A. VanOrman, H. K. Drozdick, S. Wieghold and L. Nienhaus, *J. Mater. Chem. C*, 2021, **9**, 2685–2694.

46 N. Kiseleva, P. Nazari, C. Dee, D. Busko, B. S. Richards, M. Seitz, I. A. Howard and A. Turshatov, *J. Phys. Chem. Lett.*, 2020, **11**, 2477–2481.

47 W. Chen, F. Song, S. Tang, G. Hong, Y. Wu and X. Peng, *Chem. Commun.*, 2019, **55**, 4375–4378.

48 T. C. Wu, D. N. Congreve and M. A. Baldo, *Appl. Phys. Lett.*, 2015, **107**, 031103.

49 N. Yanai, M. Kozue, S. Amemori, R. Kabe, C. Adachi and N. Kimizuka, *J. Mater. Chem. C*, 2016, **4**, 6447–6451.

50 Z. Wang and J. Zhao, *Org. Lett.*, 2017, **19**, 4492–4495.

51 N. Kiseleva, M. A. Filatov, M. Oldenburg, D. Busko, M. Jakoby, I. A. Howard, B. S. Richards, M. O. Senge, S. M. Borisov and A. Turshatov, *Chem. Commun.*, 2018, **54**, 1607–1610.

52 Z. Wang, J. Zhao, M. Di Donato and G. Mazzone, *Chem. Commun.*, 2019, **55**, 1510–1513.

53 Y. Dong, A. A. Sukhanov, J. Zhao, A. Elmali, X. Li, B. Dick, A. Karatay and V. K. Voronkova, *J. Phys. Chem. C*, 2019, **123**, 22793–22811.

54 H. Liang, S. Sun, M. Zafar, Z. Yuan, Y. Dong, S. Ji, Y. Huo, M.-D. Li and J. Zhao, *Dyes Pigm.*, 2020, **173**, 108003.

55 Y. Dong, A. Elmali, J. Zhao, B. Dick and A. Karatay, *ChemPhysChem*, 2020, **21**, 1388–1401.

56 Y. Hou, J. Liu, N. Zhang and J. Zhao, *J. Phys. Chem. A*, 2020, **124**, 9360–9374.

57 M. A. Filatov, S. Karuthedath, P. M. Polestshuk, S. Callaghan, K. J. Flanagan, M. Telitchko, T. Wiesner, F. Laquai and M. O. Senge, *Phys. Chem. Chem. Phys.*, 2018, **20**, 8016–8031.

58 J. T. Buck, A. M. Boudreau, A. DeCarmine, R. W. Wilson, J. Hampsey and T. Mani, *Chem*, 2019, **5**, 138–155.

59 D. Meroni, A. Monguzzi and F. Meinardi, *J. Chem. Phys.*, 2020, **153**, 114302.

60 V. Gray, D. Dzebo, A. Lundin, J. Alborzpour, M. Abrahamsson, B. Albinsson and K. Moth-Poulsen, *J. Mater. Chem. C*, 2015, **3**, 11111–11121.

61 J. P. Cerón-Carrasco, D. Jacquemin, C. Laurence, A. Planchat, C. Reichardt and K. Sraïdi, *J. Phys. Org. Chem.*, 2014, **27**, 512–518.

62 M. A. Filatov, S. Karuthedath, P. M. Polestshuk, S. Callaghan, K. J. Flanagan, T. Wiesner, F. Laquai and M. O. Senge, *ChemPhotoChem*, 2018, **2**, 606–615.

63 M. A. Filatov, *Org. Biomol. Chem.*, 2020, **18**, 10–27.

64 Y. Hou, I. Kurganskii, A. Elmali, H. Zhang, Y. Gao, L. Lv, J. Zhao, A. Karatay, L. Luo and M. Fedin, *J. Chem. Phys.*, 2020, **152**, 114701.

65 W. Zhao and F. N. Castellano, *J. Phys. Chem. A*, 2006, **110**, 11440–11445.

66 X.-F. Zhang, X. Yang, K. Niu and H. Geng, *J. Photochem. Photobiol., A*, 2014, **285**, 16–20.

67 Y. Y. Cheng, B. Fückel, T. Khoury, R. G. C. R. Clady, M. J. Y. Tayebjee, N. J. Ekins-Daukes, M. J. Crossley and T. W. Schmidt, *J. Phys. Chem. Lett.*, 2010, **1**, 1795–1799.

68 N. A. Durandin, J. Isokuortti, A. Efimov, E. Vuorimaa-Laukkanen, N. V. Tkachenko and T. Laaksonen, *J. Phys. Chem. C*, 2019, **123**, 22865–22872.

69 W. Sun, A. Ronchi, T. Zhao, J. Han, A. Monguzzi and P. Duan, *J. Mater. Chem. C*, 2021, **9**, 14201–14208.

70 Y. Wei, Y. Wang, Q. Zhou, S. Zhang, B. Zhang, X. Zhou and S. Liu, *Phys. Chem. Chem. Phys.*, 2020, **22**, 26372–26382.

71 V. Gray, A. Dreos, P. Erhart, B. Albinsson, K. Moth-Poulsen and M. Abrahamsson, *Phys. Chem. Chem. Phys.*, 2017, **19**, 10931–10939.

72 C. Ye, V. Gray, J. Mårtensson and K. Börjesson, *J. Am. Chem. Soc.*, 2019, **141**, 9578–9584.

73 C. Ye, V. Gray, K. Kushwaha, S. Kumar Singh, P. Erhart and K. Börjesson, *Phys. Chem. Chem. Phys.*, 2020, **22**, 1715–1720.

74 D. G. Bossanyi, Y. Sasaki, S. Wang, D. Chekulaev, N. Kimizuka, N. Yanai and J. Clark, *JACS Au*, 2021, **1**, 2188–2201.